Polymer 168 (2019) 185–198

Contents lists available at ScienceDirect

Polymer

journal homepage: www.elsevier.com/locate/polymer

Synthesis and photophysical properties of copolyfluorenes for light-emitting applications: Spectroscopic experimental study and theoretical DFT consideration

Ruslan Yu Smyslov[a,b,*], Felix N. Tomilin[c,d], Irina A. Shchugoreva[c], Galina I. Nosova[a], Elena V. Zhukova[a], Larisa S. Litvinova[a], Alexander V. Yakimansky[a,e], Ilya Kolesnikov[e], Igor G. Abramov[f], Sergei G. Ovchinnikov[c,d], Paul V. Avramov[g]

[a] Institute of Macromolecular Compounds, Russian Academy of Sciences, Bolshoy 31, St. Petersburg, 199004, Russian Federation
[b] Petersburg Nuclear Physics Institute of NRC "Kurchatov Institute"mkr. Orlova roscha 1, Gatchina, Leningrad region, 188300, Russian Federation
[c] Siberian Federal University, Svobodny 79, Krasnoyarsk, 660041, Russian Federation
[d] Kirensky Institute of Physics, Federal Research Center "Krasnoyarsk Science Centre", Siberian Branch of the Russian Academy of Science, Akademgorodok 50/38, Krasnoyarsk, 660036, Russian Federation
[e] St. Petersburg State University, Universitetskaya nab.7/9, St. Petersburg, 199034, Russian Federation
[f] Yaroslavl State Technical University, Moskovskii 88, Yaroslavl, 150023, Russian Federation
[g] Department of Chemistry and Green-Nano Materials Research Center, Kyungpook National University, 80 Daehakro, Bukgu, Daegu, 41556, Republic of Korea

HIGHLIGHTS

- Light-emitted copolyfluorenes were obtained using Suzuki and Yamamoto reactions.
- Yamamoto coupling leads in the microblock chain structure of conjugated polymer.
- Suzuki coupling allows the alternating comonomeric copolyfluorene chain.
- End groups rule photoluminescence properties of copolyfluorenes.
- Naphthalbenzimidazole group provides FRET from fluorene to Nile red.

ARTICLE INFO

Keywords:
Suzuki cross-coupling
Yamamoto polycondensation
Density functional theory

ABSTRACT

Using Suzuki and Yamamoto coupling reactions, copoly-(9,9-dioctylfluorenes) (**CPF**) were synthesized and compared regarding their photophysical properties using the spectroscopic and *ab initio* DFT approaches. The CPFs were functionalized by benzo [2,3,5] thiadiazole (**BT**) or carbazole-3,6-diyl (3,6-Cz). The latter was used to introduce different luminophore fragments, including Nile red and 4-pyrrolidinyl-1,8-naphthalimide derivatives. The effect of the two synthesis techniques on the polymer microstructure, the influence of embedding of 3,6-Cz moieties in the polymer backbone on polymer structuring, and the impact of the end groups like novel quinoxaline-containing compounds on the luminescent properties of CPFs were investigated. By comparing electron density distribution using the *ab initio* DFT approach with photoluminescence, it was shown that Suzuki reaction provides a chain microstructure with individual BT fragments separated by 9,9-dioctylfluorene monomeric units, while Yamamoto reaction leads to the blocks of BT units. This effect leads to different CPF photophysical properties (absorption and emission spectra).

1. Introduction

The development of devices for conversion of chemical or chemical-biological effects into electrical or optical signals is an urgent scientific and engineering problem. Such devices can be used in environmental protection, safety engineering, laboratory investigations, express

* Corresponding author. Institute of Macromolecular Compounds, Russian Academy of Sciences, Bolshoy 31, St. Petersburg, 199004, Russian Federation.
E-mail addresses: urs@macro.ru (R.Y. Smyslov), felixnt@gmail.com (F.N. Tomilin), shchugorevai@mail.ru (I.A. Shchugoreva), klengi49@gmail.com (G.I. Nosova), zukovaev@mail.ru (E.V. Zhukova), larissa_litvinova@hotmail.com (L.S. Litvinova), yakimansky@yahoo.com (A.V. Yakimansky), ilya-kolesnikov@mail.ru (I. Kolesnikov), abramovig@ystu.ru (I.G. Abramov), sgo@iph.krasn.ru (S.G. Ovchinnikov), paul.avramov@gmail.com (P.V. Avramov).

https://doi.org/10.1016/j.polymer.2019.02.015
Received 9 December 2018; Received in revised form 6 February 2019; Accepted 8 February 2019
Available online 10 February 2019
0032-3861/

analysis, and in designing analyzers for robototronics and different types of electronic equipment. In order to solve these tasks, it is necessary to obtain appropriate materials and develop physicochemical approaches to their synthesis. Light-emitting polymers (**LEPs**), which emit complementary colors with controlled chromaticity coordinates under low voltage, attract much attention of researchers due to the problems mentioned above. The LEPs include a class of conjugated polymers, which are presented by copolyfluorenes (**CPFs**). The latter ones have been applied in optoelectronic devices, including light-emitting diodes [1], field-effect transistors [2], and polymer solar cells [3,4]. Also, they can be used in the fabrication of chemo- and biosensors for detecting explosive agents and cation-anion compositions and for molecular biology applications [5–7].

The semiconductor properties (hole- and electron-type conductivity) of copolymers offer extensive opportunities for engineering applications of these materials. Such polymers can improve the process of fabrication of optoelectronic devices and exhibit desirable photophysical characteristics [8]. The high operation efficiency of CPF-based optoelectronic devices can be obtained by embedding additional luminophores together with an electron-transport component [9]. In the CPF films of specific compositions, the Förster resonance energy transfer (**FRET**) of electron excitation to the conjugated fluorene-benzo [2,3,5]thiadiazole-fluorene (**F-BT-F**) fragments takes place. This effect manifests itself in the increased brightness and efficiency of green electroluminescence (**EL**) [9]. In macromolecular design, it is essential to correctly select the amount and quality of luminophores, transport components, and polymer end groups. The CPFs form the most promising class of conjugated polymers, which can be tuned to radiation over the entire visible spectral range. It is of great importance for designing single-layer white radiation sources [10,11].

The chemical design of CPFs requires to take into account the conformational changes in the polymer chain, which depend on the type and density of side grafting. The side fragments also determine the solubility of polymers in different media, including water and alcohols. Many fluorescent chemosensors are based on the photoinduced electron transport to the polymer backbone: their conjugation enhances quenching due to the energy migration along the polymer circuit [12]. Therefore, it is essential to control the electron excitation energy transfer (**EET**) both along the polymer chain and between the macromolecules.

The CPFs were functionalized by carbazole-3,6-diyl (**3,6-Cz**) comonomer units, which were used to introduce the luminophore groups of Nile red (**NR**) and 4-pyrrolidinyl-1,8-naphthalimide (**NI**) derivatives in the CPF pendants. Embedding of such 3,6-Cz fragments in the CPF backbone ensures controlling of aggregation in a polymer film and makes it possible to improve the balance between electron and hole carriers. The advantage of the 3,6-Cz-based monomers over the 2,7-Cz-based ones is the simplicity of formation of the former. It should be taken into account that 3,6-Cz units in contrast to 2,7-Cz ones deteriorate the π-conjugation along the CPF chain [13].

NR is a well-known luminescent label characterized by a high quantum yield, which was successfully used in the fabrication of organic LEPs by diffusion to the light-emitting layer using a mask for forming a trichromatic device [14]. However, NR is rarely used in polymers with covalent attachment. As was shown in Ref. [13], it often poorly emits in EL spectra of CPFs, which is determined by the copolymer environment and composition, while in CPF photoluminescence (**PL**) spectra it is sufficiently active if the effective EET is provided. NR broadens the LEP emission range and makes it possible to cover the PL range from 550 to 620 nm. In this work, Nile Red was used as a red luminophore component of the CPFs, which can be applied in designing of chemo- and biosensors.

The blue-green luminescent component used was 3,6-Cz monomeric units with NI in their pendants. The NI-containing fragment is characterized by a high quantum yield, as well as by both electron and hole conductivity, which is important for EL.

The luminophore and transport fragments with the electron- and hole-type mobility of free carriers or receptor and sensor-active groups embedded in the macromolecule affect the operation efficiency of various LEPs. Besides, terminal Br or borolane reactive groups may lead to electrochemical oxidation of CPFs synthesized via Suzuki polycondensation and even degradation of electrodes. Therefore, in designing CPF chemical structures, it is critical to correctly choose the end groups that will replace the aforementioned reactive groups in the final synthesis stage, prevent charge recombination near electrodes, and facilitate charge transport to the central part of the emission layer [15,16]. It should be taken into account that sometimes the introduced end groups may play the role of traps for both carriers (electrons and holes) and excitons at the EET [17]. Since the range of readily available and easily introducible end groups is not very broad, it is important to augment it by new end group structures, e.g., earlier undescribed electron-acceptor quinoxaline-containing compounds.

Embedding new structures in polyfluorene, one should take into account their possible effect on the formation of ordered (*β*) phases (or H and J aggregates) in CPF, which are typical in polyfluorene and may influence the properties of LEPs [18–20].

It was previously shown that, depending on the synthesis method used — Suzuki or Yamamoto cross-coupling, copolymers based on fluorene (**F**) and benzo [2,3,5] thiadiazole (**BT**) have different photoluminescent properties [21]. This study aims to find out with the help of quantum-chemical calculations (absorption and emission spectra and oscillator strength), what this effect is connected with, and also to optimize the molecular design of conjugated light-emitting polymers taking into account the influence of end groups. So in this work, CPFs with quinoxaline end groups with donor-acceptor properties were first synthesized.

2. Experimental

2.1. Materials

The catalysts tetrakis (triphenylphosphine)] palladium (0) and bis (1,5-cyclooctadiene) nickel (0) and the monomers 3,6-dibromocarbazole, 2,7-dibromofluorene, 4,7-dibromo-2,1,3-benzothiadiazole, and 9,9-diocty-2,7-bis (trimethyleneborate) fluorene were obtained from Sigma Aldrich and used as received.

2.2. Synthesis

2.2.1. Synthesis of monomers and copolymers

The CPFs were prepared via Suzuki–Miyaura cross-coupling reaction of 9,9-dioctyl-2,7-bis(trimethyleneborate)fluorene monomers with 2,7-dibromo-9,9-dioctylfluorene with required dibromo-derivatives of aromatic comonomers or via Yamamoto polycondensation of dibromo-derivatives of aromatic comonomers (Fig. 1). Either 4,7-dibromo-2,1,3-benzothiadiazole (P1−P3, *see* Fig. 2, Table 1) or NI derivative N-[6-(3,6-dibromocarbazol-9-yl)hexyl]-[(4-pyrrolidine)-1-yl]-1,8-naphthalimide were used as green luminophores in backbone or side chains of P4 and P5 polymers. The derivatives of 3,6-Cz and NR comonomer N-[6-(3,6-dibromocarbazole-9-yl)hexyloxi-9-diethylamino-H-benzo [α] phenoxazine-5-on] comonomers were used as red luminophores in polymers P6–P9.

The polymers were functionalized by embedding substituents in 3,6-dibromocarbazole through a spacer hexamethylene group. The Suzuki and Yamamoto coupling reactions occurred either upon thermal heating (P1–P8) or in a microwave reactor (P9–P14, P14 (R_1) – poly-(9,9-dioctyl)fluorene). The use of microwave irradiation as an alternative heat source allowed one to reduce the polymer synthesis time by a factor of more than 10 relative to the conventional time. Various Br-derivatives of aromatic compounds (R1–R8) were embedded in the polymers as end groups at the final reaction stages.

The monomer and polymer synthesis (under thermal heating for

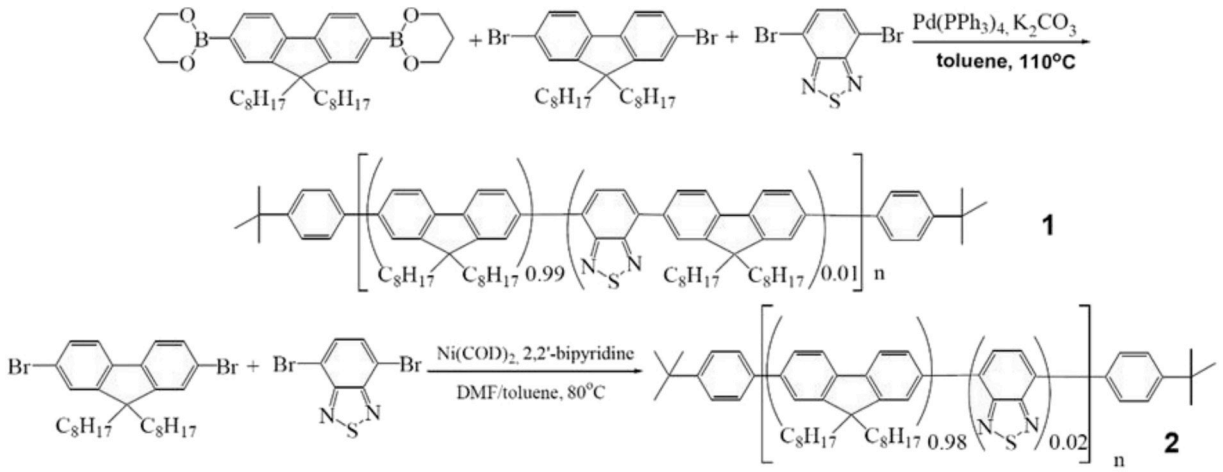

Fig. 1. Schematic of synthesis of the CPFs with the 2,1,3-benzothia [2,3,5]diazole fragments: Suzuki (1) and Yamamoto (2) polycondensation.

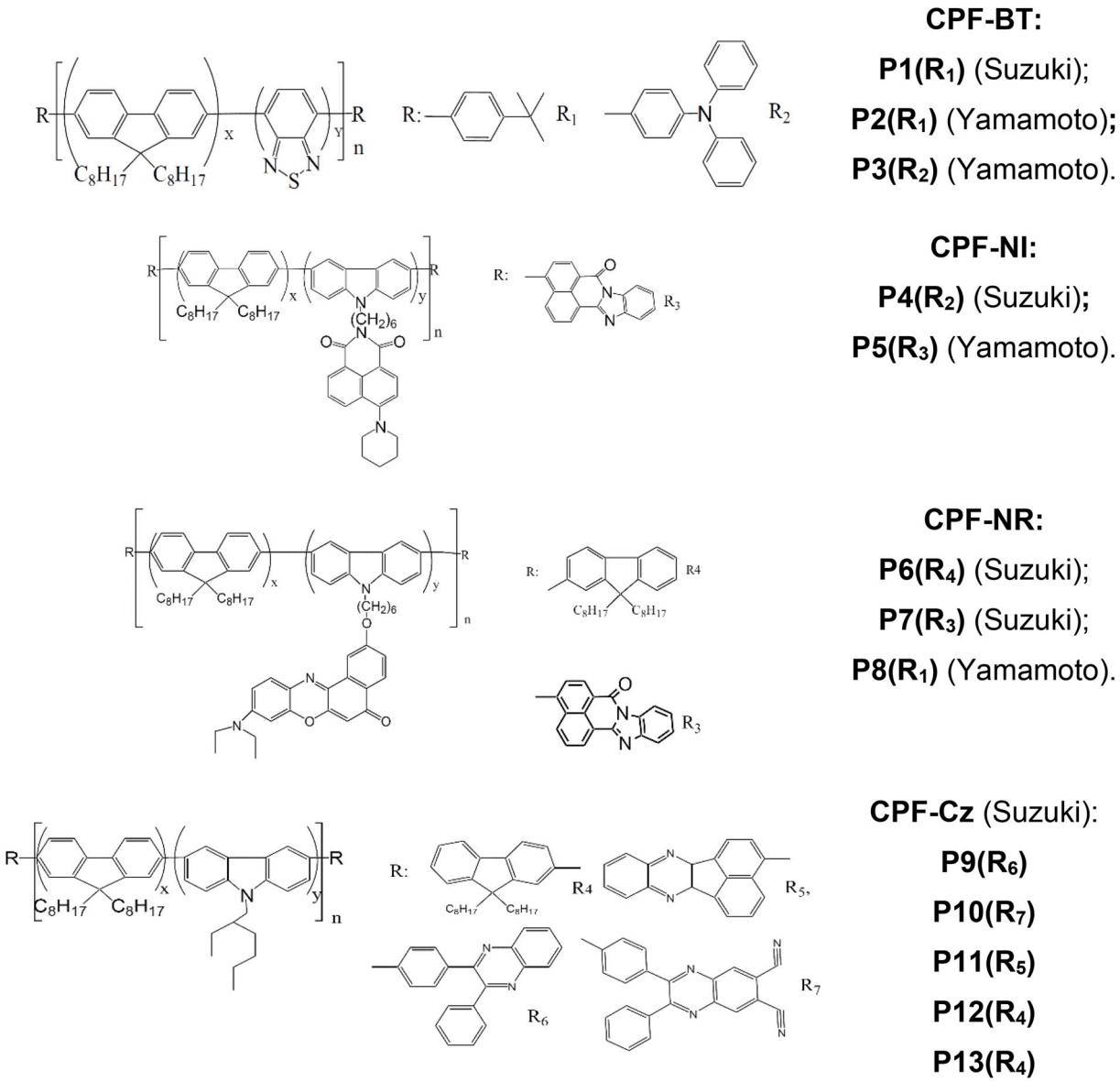

Fig. 2. Chemical formulae of synthesized CPFs P1−P13, indicating the contents of fluorene and co-monomeric unit in a polymeric chain of CPF in amounts of x and y, respectfully, and the end groups used.

Table 1
Composition and properties of the synthesized copolyfluorenes.

Polymer[a]	Composition[b]			GPC-PS[c]		GPC-LS-RI-VS[d]		PL chromaticity coordinates xyCIE 1931	Quantum yield PL[g], φ, %
	x, mol.%	y, mol.%	end group	$M_w \cdot 10^{-3}$[e]	$Đ_M$[f]	$M_w \cdot 10^{-3}$	$Đ_M$		
P1	99.00	1.00	R_1	43.7	2.30	22.0	1.72	0.353, 0.573	35.81
P2[h]	98.00	2.00	R_1	73.8	2.50	33.4	1.60	0.391, 0.382	20.54
P3[h]	98.00	2.00	R_2	47.8	2.20	24.8	1.51	0.430, 0.400	19.00
P4	99.00	1.00	R_2	50.1	2.60	25.3	1.94	0.192, 0.414	27.62
P5[h]	99.00	1.00	R_3	177.4	2.70	79.8	2.00	0.205, 0.236	10.56
P6	98.80	1.20	R_4	17.3	1.89	30.0	1.67	0.399, 0.335	4.24
P7	99.85	0.15	R_3	37.1	2.51	19.9	1.80	0.333, 0.427	14.81
P8[h]	99.85	0.15	R_1	114.0	2.70	51.2	1.72	0.348, 0.293	11.79
P9[i]	97.50	2.50	R_6	52.9	1.84	24.9	1.44	0.190, 0.158	9.96
P10[i]	90.00	10.00	R_7	57.8	1.93	29.9	1.53	0.436, 0.464	10.45
P11[i]	90.00	10.00	R_5	57.8	1.93	16.9	1.36	0.193, 0.305	9.94
P12[i]	97.50	2.50	R_4	101.3	2.46	38.7	1.77	0.185, 0.136	25.04
P13[i]	90.00	10.00	R_4	71.7	2.24	33.6	1.59	0.195, 0.164	10.41
P14[i]	100.00	0.00	R_1	78.2	2.32	33.5	1.71	0.168, 0.104	15.53

Notes:
[a] P1−P8 films were prepared by casting of CPF solution in chloroform onto glass and P9–P14 ones were prepared by spin-casting polymeric solutions in toluene.
[b] Note here x and y are the contents of fluorene and co-monomeric unit, respectfully, in a polymeric chain of CPF. See these moieties and end groups, R, in Fig. 2.
[c] The gel permeation chromatography with PS calibration.
[d] The gel permeation chromatography with multiple detection using light scattering, refractive index, and viscosimetry.
[e] The mass-average molar mass (or molecular weight).
[f] The dispersity difined as $Đ_M = M_w/M_n$, where M_n is the number-average molar mass (or molecular weight).
[g] The PL quantum yield is given for the CPF films.
[h] The polymers were prepared by the Yamamoto method.
[i] Poly-(9,9-dioctyl)fluorene was prepared by microwave synthesis.

polymers P1–8) were described in Refs. [13,22]; Br-derivatives of quinoxalines were synthesized via the technique proposed in Ref. [23]. CPFs P9–13 were obtained under microwave irradiation in a CEM Discover SP reactor at a magnetron frequency of 2.45 GHz. The reaction occurred under an argon atmosphere and magnetic stirring; the reaction temperature was controlled by an IR thermometer on the retort outer surface. For maintaining the reaction temperature profile, the microwave oven output power was automatically controlled using the software algorithm.

The structures of the synthesized polymers are shown in Fig. 2. The polymers have mass-average molar mass (or molecular weight) M_w = 20–177·10^3 and the heterogeneity index, or simply dispersity $Đ_M$ = 1.7–2.5. Composition and properties of the synthesized polymers are given in Table 1.

2.2.2. Synthesis of copolyfluorene P12 under microwave irradiation

A 100-ml retort with a cooler and two-valve adapter for operation in vacuum and embedding of solvents was filled with 0.2852 g (0.501 mmol) of a 9,9-dioctylfluorene-2,7-diboronic acid bis(1,3-propanediol) ester, 0.2605 g (0.475 mmol) of 9,9-dioctyl-2,7-dibromofluorene, and 0.01093 g (0.025 mmol) of 3,6-dibromo-N-(2- ethylhexyl) carbazole. After removal of oxygen from the system, the system was filled with 15 mg (0.0058 mmol) of $Pd(PPh_3)_4$, repeatedly evacuated, and washed with argon. An alkali medium was the 2-M aqueous solution of K_2CO_3; the reaction occurred in the presence of Aliquat® 336 trioctylmethylammonium chloride. The retort was filled with 6 ml of toluene, 2.5 ml of the 2-M aqueous solution of K_2CO_3, and aliquot solution (25 mg in 0.7 ml of toluene). The setup was placed in a microwave oven, and the reaction solution was stirred at 100–104°C for 1.5 h (80 wt). Then, the reaction retort was added with 9,9-dioctyl-2,7-bis (trimethyleneborate)fluorene (20 mg in 1 ml of toluene) and, after heating for 40 min, with 45 mg of 2-Br-9,9-dioctylfluorene in 1.5 ml of toluene. Stirring and heating were continued for more 40 min; after that, the polymer was precipitated in methanol, filtered, repeatedly dissolved in $CHCl_3$, and precipitated in methanol again. The low-molecular polymer fractions were removed by acetone extraction in a Soxhlet extractor. The CPF yield after cleaning was 85%.

2.3. Characterization methods

2.3.1. Liquid chromatography

The molecular mass (**MM**) characteristics of the polymers (Table 1) were determined by liquid chromatography on an Agilent Technologies liquid chromatograph equipped with three detectors: refractometric, viscometric (**VS**), and light-scattering (**LS**) with styragel columns; tetrahydrofuran (**THF**) (1.0 ml/min) was used as the eluent. The MM characteristics were also calculated using calibration by polystyrene standards to compare them with the data previously obtained [24,25].

2.3.2. Photoluminescence and absorption UV–visible spectroscopy

Assessment of the degree of occurrence of functional comonomer fragments in the polymer chain by NMR is difficult because of their small amounts. The presence of luminophores was recorded by the luminescent method of polymer films. PL emission and excitation spectra for copolyfluorenes were detected on an LS-100 BASE luminescence spectrophotometer (*PTI® Lasers INC*, London—Toronto, Canada). The luminescence intensity I_{lum} was recorded in the fluorescence mode from the exciting light beam incidence side in the phosphorescence mode using a solid-sample holder. The grazing angle between the exciting light beam and a sample was ~30°. The emission spectra wavelength range was 400–750 nm at an excitation wavelength of λ_{exc} = 380 nm; for the excitation spectra, the span was 210–400 nm at a luminescence observation wavelength of λ_{em} = 430 nm. The spectral widths of excitation and luminescence monochromator slits were 5 and 2 nm; the PMT gain was 500. For the sake of comparison, the I_{lum} values were reduced to an internal laboratory standard. Absorption spectra were detected on an SF-256 UVI spectrophotometer (LOMO Fotonika, St. Petersburg, Russia).

The photoluminescence quantum yield (**PLQY**) of the polymers was measured by the modified de Mello method using a Fluorolog-3 fluorescence spectrometer equipped with a Quanta-j integrating sphere [26]. Samples were deposited onto glass substrates by spin-coating from toluene. In determining the PLQY, a clean substrate was used for comparison. All the measurements were performed at room temperature.

For studying PL and absorption spectra, the CPF layers were formed by spin-coating on the glass from toluene solutions or by CPF casting in

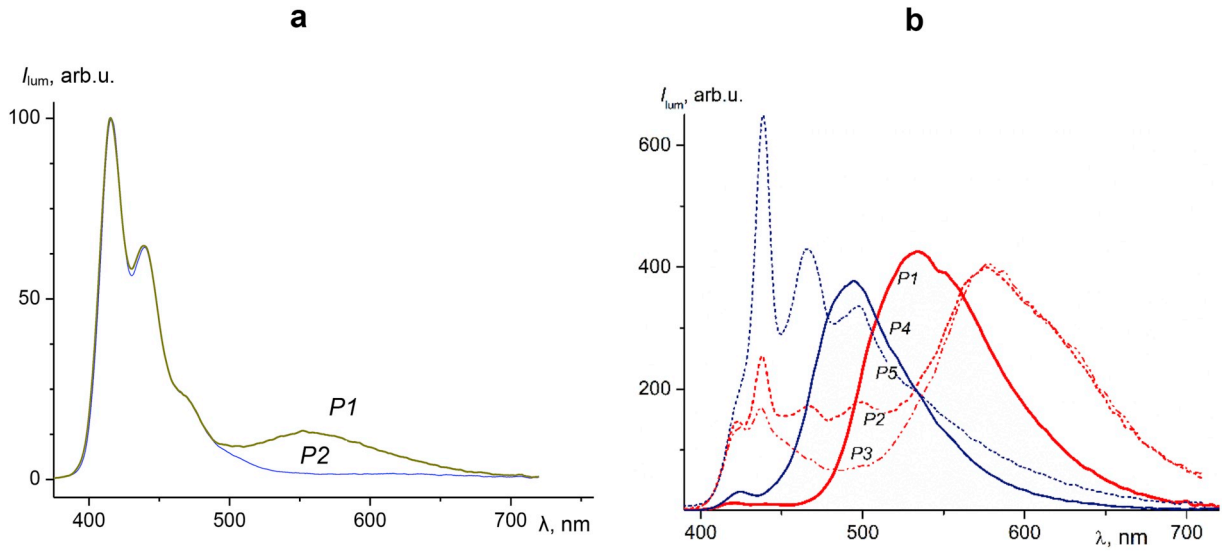

Fig. 3. Photoluminescence spectra for the CPFs in chloroform (a) for **P1** and **P2** and for the films (b) for **P1** – **P5** upon excitation at 380 nm.

chloroform (P1–P8). The CPF solution concentration was 10 mg/ml.

2.4. Quantum-chemical calculations

The geometry of all the simulated structures was optimized using a hybrid exchange-correlation B3LYP functional [27,28] with 6–31G (d, p) basis set [29] in the framework of the density functional theory (**DFT**) [30] in the gas phase. Absorption spectra were calculated by time-dependent density-functional theory (**TD-DFT**) using 6-31G (d, p) basis. For calculating the emission wavelength, the geometry of the molecules was optimized in the excited states at TD/B3LYP/6-31G (d, p) level of theory. The solvent effects in absorption and luminescence spectra have been described within the polarizable continuum model (**PCM**) [31]. All calculations were performed using the GAMESS code [32].

3. Results and discussion

3.1. Photoluminescence of copolyfluorenes

To choose an optimal CPF synthesis technique, we compared the PL spectra of CPFs synthesized via Suzuki and Yamamoto polycondensation reactions to ensure the most predictable polymer properties. The PL spectra of CPF with benzothiadiazole units in the CPF backbone are presented in Fig. 3a (for **P1** and **P2**) and Fig. 3b (for **P1**—**P3**). The PL spectra of NI-containing and NR-containing luminophore comonomers in the polymer chain are presented in Fig. 3b (for **P4** and **P5**) and Fig. 4 (for **P6**—**P8**), respectively. Despite a low luminophore (comonomer) content, the luminescent properties of polymers **P1**—**P8** prepared by different methods appeared to be substantially different in both dilute solutions and films.

The most significant changes were observed upon embedding the BT units in the macromolecule backbone, which is confirmed by literature data [9,22,33]. In particular, in the Yamamoto synthesis, embedding of the *N*-phenyl-1,8-naphthalimide (0.5–3.0%, λ_{pl} = 500 nm) luminophore as end groups and BT units (2–3%) in the backbone yielded a CPF PL spectrum with the emission similar to the achromatic color. In such a way, the chromaticity coordinates according to the grading scale of the International Commission on Illumination 1931 (**xy CIE1931**) were found to be (0.31; 0.39), and the maximum brightness was 50–251 cd/cm^2 (Ca/Ag cathode) [22]. The emission band contained a maximum at 580 nm (orange color shade). At the same time, embedding of BT fragments to the backbone of the polymers synthesized using the Suzuki

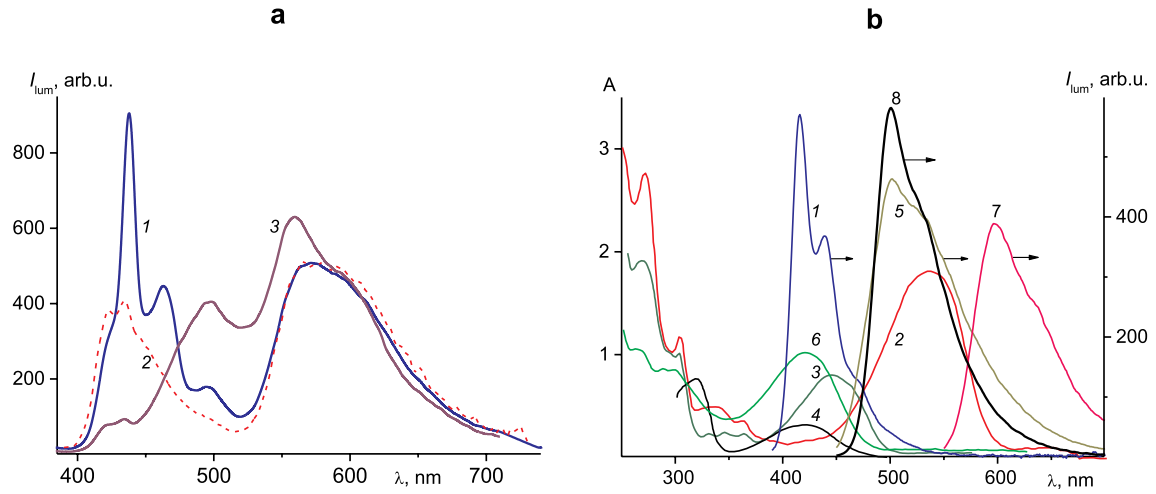

Fig. 4. Emission spectra of the films (a) for **CPF-NR: P8** (*1*), **P6** (*2*), and **P7** (*3*) and spectra in chlorophorm (b): emission spectra (*1, 5, 7, 8*) and absorption spectra (*2, 3, 4, 6*) for poly (9,9-dioctyl)fluorene (*1*), 2-[6-(3,6-dibromocarbazole-9-il)-hexyloxi]-9-diethylamino-5H-benzo [α] phenoxazine-5-on (*2, 7*) and N-[6-(3,6-dibromocarbazole-9-il)-hexyl]-[(4-pyrrolidine)-1-il]-1,8-naphthalimide (*3, 8*) monomers, and model compounds F-BT-F (*4*) and NBI-F-NBI (*5, 6*). $c_{pol} = 10^{-5}$ mol/L.

method leads to the green EL emission [9,33].

Study of the electrooptical [21] and PL properties of chloroform solutions of the synthesized CPFs with the BT monomeric units showed that the use of different synthesis methods leads to the differences in molecular microstructures of these copolymers. The Suzuki reaction (**P1**) ensures the distribution of BT units in the form of F-BT-F sequences in the poly (9,9-dioctyl)fluorene chain at distances comparable with the conjugation length (5–6 monomeric units). Study of the PL properties of polymers synthesized using the Yamamoto reaction (**P2**) showed the possibility of formation of the F-BT-BT-F blocks. The absorption and PL spectra of chloroform CPF films solutions did not show the fluorene band redshift. Two vibronic peaks at 427 and 448 nm were identified, which are indicative of emission of a film with a relatively disordered structure related most likely to the α-phase of a Gaussian polymer coil [34,35].

The EET in isolated copolymer molecules, which is only observed in copolymer **P1**, occurs directly at the F-BT unit contact; this polymer should have more such contact bonds than copolymer **P2** (Fig. 3a). The PL spectrum of copolymer **P2** does not show any noticeable energy transfer from fluorene to the BT chromophores. The concentration of the F-BT contact units in isolated molecules of **P2** is insufficient to provide such energy transfer. In films of these CPFs, the high-efficiency intermolecular FRET occurs. An almost complete energy transfer from CPFs **P1** (1 mol% of BT) leads to the green emission with λ_{max} = 540 nm, which is characteristic of a model F-BT-BT-F compound (curve *4* in Fig. 4b; λ_{abs} = 425 nm, λ_{max} = 535 nm is not shown).

The PL spectra of copolymers **P2** and **P3** with 2 mol% of the BT units synthesized by the Yamamoto method (Fig. 3b) contain bands typical for polyfluorene and a broad band in the orange spectral range with λ_{max} = 570 nm, which can be caused by the formation of the F-BT-BT-F blocks. This band arises in the film spectrum due to the conformational variations at the transition from the solution to the film phase (packing), the twist angle between fluorene units being reduced [20]. An approach of macromolecular segments results in the intermolecular excitation energy transfer from fluorene units to the formed BT-BT blocks. The differences between PL spectra near 500 nm can be caused by the effect of different end groups. Triphenylamine groups ($\mathbf{R_2}$), in contrast to 4-tret-butylphenyl groups ($\mathbf{R_1}$), can prevent the formation of terminal excimers and significantly reduce the cyan or green emission of fluorene segments (P2 and P3, or P5 and P4 in Fig. 3b) [36]. The results show that the use of monomers with the different reactivity of functional groups leads to the formation of blocks in a macromolecular chain during the Yamamoto synthesis.

An OLED device based on **P1** emits green light: the xyCIE1931 coordinates are (0.316, 0.507) with the maximum brightness of 4000 cd/m^2 at 10 V. The respective values for polymer **P2** are (0.276, 0.274) and 3750 cd/m^2, which corresponds to the near-white EL [21]. The change of 4-*t*-butylphenyl end groups for the triphenylamine groups (**P3**) leads to the change of the chromaticity coordinates xyCIE1931 (0.377; 0.356) for OLEDs with the ITO/PEDOT:PSS(50 nm)/CPF (50–60 nm)/Ca (50 nm)/Al (100 nm) configuration.

Upon embedding the 3,6-Cz (1 mol.%) comonomeric fragments, containing NI luminophore group pendants – **P4($\mathbf{R_2}$)** and **P5($\mathbf{R_3}$)** – to the CPF backbone, the formation of blocks can also occur in the polymer synthesis by the Yamamoto method. In this case, the copolymer **P5** contained an additional naphthalbenzimidazole (**NBI**) luminophore end group R_3, which is luminescent in the same range as **NI** (curves *5* and *8* in Fig. 4b). The polymer microstructure variation is indicated by a weak emission intensity contribution in the fluorene band region *ca.* 424 nm in **P4** synthesized by the Suzuki method and the change in the ratio between the peaks at 466 and 495 nm in comparing with polymer **P5** by the Yamamoto method (see in Fig. 3b). So, the structural modifications (the block structure F-Cz-Cz-F of carbazole fragments and appropriate packing in the polymer) lead to the incomplete EET from fluorene to the **NI** fragments, in contrast to polymer **P4** synthesized using the Suzuki method (compare curves for P4 and P5 in Fig. 3b). The indices xyCIE1931 (0.192, 0.414) of the **P4** emission correspond to the green color. It is worth noting that the maximum intensity corresponding to the **NI** fragment in the emission band at 495 nm does not change in the film and solution and corresponds to the monomer PL (curve *8* in Fig. 4). Polymer **P5** luminesces mainly in the blue spectral range with xyCIE1931 (0.205, 0.236), which is consistent with the literature data [37] and the incomplete EET mentioned above.

NR-containing CPFs **P6** (1.2 mol% of NR) and **P8** (0.15 mol% of NR) were synthesized using two techniques. They have no characteristic differences in the NR spectral range (530–700 nm, l_{max} = 576 nm) (curves *1* and *2* in Fig. 4a) probably due to the low luminophore content in polymer P8. The NR band maximum in the film is shifted by 15 nm relative to the polymer and monomer solution in $CHCl_3$ (curve *7* in Fig. 4b), which is indicative of the effect of environment on the dye PL in the solid state. As the NR concentration increases from 0.15 (**P7**) to 1.2 mol% (**P6**), the fluorene band intensity in the range of 400–510 nm decreases, which is related to an increase in the efficiency of EET to NR. However, a weak overlap of the NR absorption band (450–640 nm, l_{max} = 538 nm) with **PF** emission (curves *2* and *7* in Fig. 4b) deteriorated FRET conditions as compared with the case of the CPF containing the **BT** or **NI** units (curves *3*, *4*, and *6*). Polymer **P7** synthesized by the Suzuki method carries a luminescent NBI end group, to which the EET from the 9,9-dioctylfluorene unit entirely occurs because of the overlap of the absorption and emission bands (compare curves *1* and *3* or *6*). Then, the electron excitation energy migrates from NBI to 0.15 mol% of NR (compare curves *2* and *5* in Fig. 4a and curves *1* and *2* or *3* in Fig. 4a).

The results show that embedding of 1 mol% of the comonomeric units to the backbone in the Yamamoto synthesis (in comparison with the Suzuki method) leads to the formation of block structures F-Cz-Cz-F and the EET in the films becomes less efficient due to structural changes.

The CPF aggregation at the transition from the solution to the films facilitates the formation of excimers and exciplexes and plays a key role in PL. The electron density delocalization effect manifests itself in the PL band broadening due to the strong intermolecular interactions (compare curves *1*(a) and *7*(b) in Fig. 4). In this case, the effect of solvent polarity is exhibited in the stabilization of the chromophore excited state: a bathochromic shift in the PL spectrum is observed. In addition, it was shown that, regardless of the synthesis technique used, the EET in the solid state is significantly affected by the end groups. To investigate the effect of embedding of 2.5 and 10 mol% of the 3,6-Cz comonomeric groups in the poly (9,9-diactyl)fluorene backbone on the polymer structure, we synthesized CPFs P12 and P13 in a microwave reactor by the Suzuki method. The obtained polymers were used to study the effect of the previously unknown quinoxaline-containing end groups (R_5—R_7) on luminescence of CPF **P9–P11**. The films were spin-cast from the polymer solutions in toluene. It should be noted that the homopolymer **P14** and carbazole-containing polymers **P12** and **P13** had similar emission band profiles with l_{max} at 435, 460, and 495 nm (Fig. 5a).

The PL spectrum shift to the red spectral range and change in the ratio between the fluorene bands observed at the transition from chloroform to toluene can be related to aggregation processes, i.e., the formation of the β phase with the characteristic maximum in the emission band at 435 nm [19, 38–42]. At the same time, as was shown in the literature [37,40,41], embedding of the 3,6-Cz units reduces the polymer chain conjugation length and aggregation.

In the spectra of polymers **P12** containing 2.5 mol% of 3,6-Cz units, an additional shoulder at 410–440 nm is observed in the absorption band of 340–450 nm with the maximum of *ca.* 390 nm. Since this shoulder is also pronounced for poly-(9,9-dioctyl)fluorene (**P14**) prepared under like conditions, it can be attributed to the presence of the β phase in the CPF. It was found that an increase in the 3,6-Cz-unit content from 2.5 to 10% leads to the disappearance of the shoulder at 410–440 nm in the CPF absorption spectra (curves *2* and *3* in Fig. 5a).

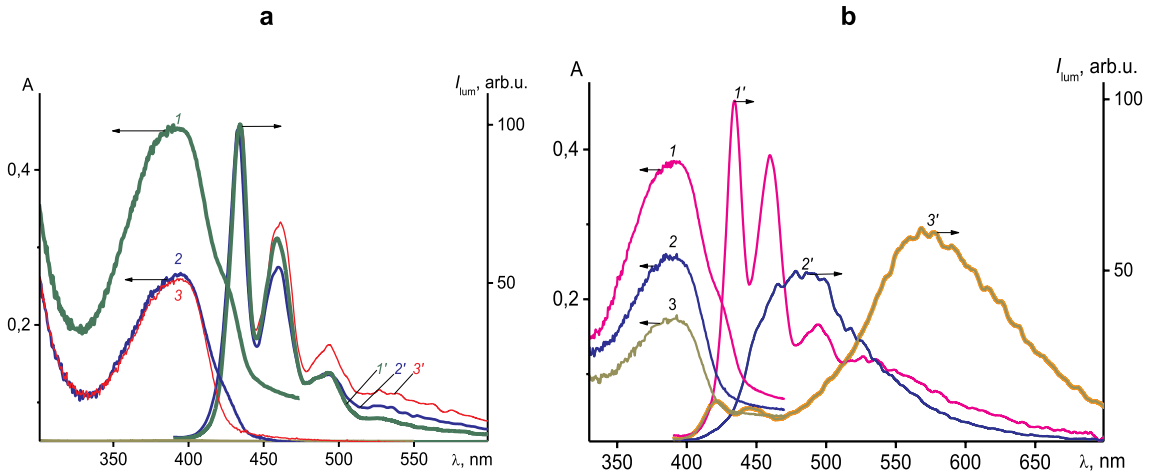

Fig. 5. Absorption (*1–3*) and emission (*1′—3′*) spectra of the CPF films containing the 3,6-Cz units (**a**) for **P14** (*1, 1′*), **P12** (*2, 2′*), and **P13** (*3, 3′*) and quinoxaline end groups (**b**) for **P9** (*1, 1′*), **P11** (*2, 2′*), and **P10** (*3, 3′*) upon excitation at 380 nm. Spectra in Fig. 5a are normalized at 435 nm.

This effect can be interpreted as the destruction of the *β* phase with increasing content of comonomer units above the critical value. It could be expected since the 3,6-Cz unit content concerning the fluorene units in **P12** is 1: 39, which does not break the conjugation of the 6–10 PF units responsible for the formation of *β*-phase aggregates. However, the further growth of the 3,6-Cz unit content to a ratio of 1: 9 concerns already the conjugation length range, in accordance with the data reported in Ref. [5], from 6 to 7–10 units [43]. Then, the *α* phase of polyfluorene Gaussian coils is only retained. Thus, embedding of 10 mol % of the 3,6-Cz units in polyfluorene yields a kink in the linear polymer structure and reduces the conjugation length. The latter results in the disappearance of aggregates since they are stabilized by this conjugation and interaction between side octyl groups.

The trend of aggregation weakens, facilitating the structural stabilization of the polymer [38]. The changes in the *β*-phase content and length of the conjugated F-unit parts complexly manifest themselves as a change in the contribution of vibronic peaks with l_{max} at 435, 460, and 495 nm in the range of 400–510 nm (compare curve *1′* with curves *2′* and *3′* in Fig. 5a; curve *1′* in Fig. 5b).

Comparison of the absorption spectra in Fig. 5b for the films of quinoxaline-containing CPFs **P9** (curve *1*) as well as **P10** and **P11** (curves *2* and *3*) also demonstrated a shoulder at 410–440 nm only at a 3,6-Cz unit content of 2.5 mol% (curve *1*). Thus, the chemical nature of the end group does not noticeably affect the stabilization of *β*-phase aggregates. In this case, the CPF molecular mass (**MM**) is relatively high: MM = 52.9 kDa for **P9** (Table 1); otherwise, the *β*-phase content depends on the polymer MM and MM dispersity [39,42].

Using an example of polymer **P9-11,** we demonstrate the effect of quinoxaline end groups on the luminescent properties of the CPFs. Upon embedding of the 2,3-phenyl-quinoxaline (R_6) end group in polymer **P9** (Fig. 5b), the chromatic characteristic of polyfluorene does not noticeably change. In particular, for **P12** (by2.5%), the xyCIE value is (0.185, 0.136) and for **P9,** it is (0.190, 0.159) (Table 1 and curve *1′* in Fig. 5b). However, in the presence of nitrile groups in a quinoxaline fragment (R_7), the luminescence bands of both the reference compound R_7-F-R_7 and polymer **P10** have a maximum at 572 nm (curve *3′* in Fig. 5b). In this case, the 2,3-phenyl-quinoxaline-6,7-dicarbonitrile end group, similar to naphthalbenzimidazole (curve *3* in Fig. 4a for **P7**), is an active luminophore, to which the EET from fluorene F units (x = 0.436, y = 0.464) mainly occurs. In polymer **P11** (curve *2′* in Fig. 5b), the quinoxaline fragment is bound to the conjugated chain of F units through the acenaphtho [1,2]quinoxaline (R_5) group rather than through the phenyl core; therefore, the PL spectrum contains one band with λ_{max} = 485 nm and xyCIE1931 (0.193, 0.305). The absence of PL bands typical of a chain of conjugated F units is indicative of the energy transfer from this chain to quinoxaline end group R_5.

Table 1 gives PLQYs *φ* of the synthesized CPF thin films. The highest quantum yields (from 25 to 36%) were obtained for the CPFs synthesized via the Suzuki reaction, i.e., for **P1**, **P12**, and **P4(R_2)**. These are binary copolymers, in which the second component is BT, 3,6-Cz, and 3,6-Cz-NI, respectively. Here, it should be noted that when the polymer backbone has a BT fragment that does not break the conjugation, the quantum yield is maximum and amounts to 35%. Replacement of this fragment for the conjugation-breaking 3,6-Cz unit leads to a decrease in the quantum yield to 25%. A slight increase in the quantum yield to 27.6% for **P4(R_2)** can be attributed to the energy transfer using the overlap of the fluorescence bands of fluorene unit sequences in the backbone and absorption of the NI groups (Fig. 4b). However, when this overlap of the polymer-forming components is insignificant, as in the F and NR units in CPFs **P6** and **P7**, the quantum yield lowers to 4–15%.

The CPFs synthesized using the Yamamoto reaction also exhibit a reduction of the quantum yield from 20 to 10% at the transition from copolymers **P2** and **P3** containing the BT units to polymers **P5** and **P8** containing the NI and NR fragments. In this case, a decisive role in a decrease in the *φ* value is played again by the replacement of the BT fragments in a macromolecule for the 3,6-Cz units, which break the backbone conjugation. Also, the presence of a small amount of NR units (0.15%) leads to the quantum yield drop by a factor of 2, which is related, as we showed above, to the weak EET from the fluorene chain to the NR fragments.

The smaller quantum yield of 20% for polymers **P2** and **P3** synthesized using the Yamamoto reaction, as compared with a value of 35% for polymer **P1** synthesized using the Suzuki mechanism, is indicative of the possible formation of blocks of BT fragments in the Yamamoto reaction. For such blocks, the absorption band will be weaker overlapped by the fluorescence band of fluorene unit chains than in the case of isolated BT units in the CPF chain. This fact causes the observed ETT drop. Similarly, we can take into account the block structure consisting of 3,6-Cz units in polymer **P5** synthesized using the Yamamoto reaction and its absence in polymer **P4** synthesized via the Suzuki mechanism. The 3,6-Cz unit blocks break the conjugation of fluorene chains stronger than single 3,6-Cz units and thereby lower the efficiency of EET from the fluorene units to the NI 3,6-Cz units in **P4** relative to the case of **P5**, which is reflected in a decrease of the quantum yield from 27.6 to 10.6%. The quantum yield drop from 14.8% in **P7** to 11.8% in **P8** can be explained similarly.

In addition, it is worth noting that an increase in the amount of the second component in binary copolymers leads to a decrease in the quantum yield. For example, the NR content growth from 0.15 in **P7** to

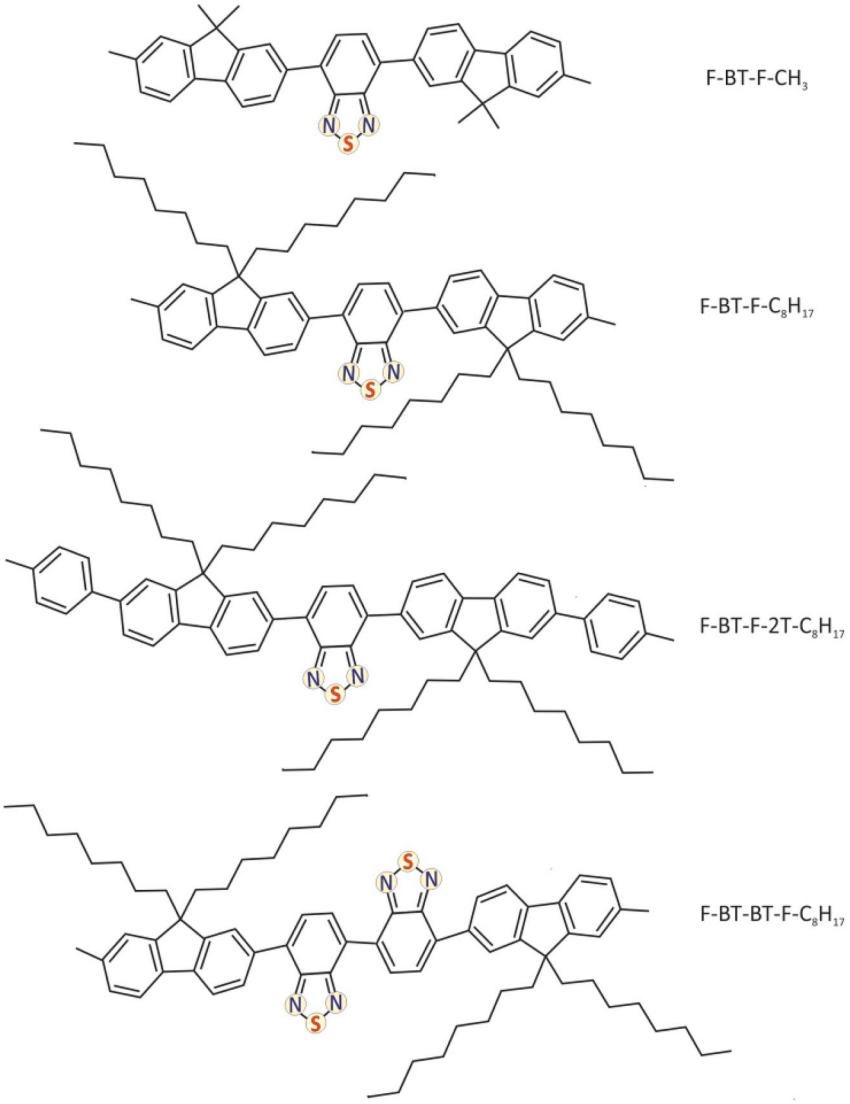

Fig. 6. Copolyfluorene models for the quantum-chemical calculation.

1.2% in **P6** leads to a sharp decrease in the φ value from 14.8 to 4.2%. The same trend is observed for polymer **P12** containing only 2.5% of the 3,6-Cz units and for polymer series **P10**, **P11**, and **P13** containing 10% of such units. In this case, the quantum yield decreases from 25 to 10%. Interestingly, copolymer **P9** contains, similar to **P12**, 2.5% of 3,6-Cz units. However, its quantum yield is as low as 10%. This result shows that the R6 end group, in contrast to R_4, is a quencher (Fig. 2).

3.2. Quantum-chemical calculations

3.2.1. Copolymer models

Using quantum-chemical calculations, the structural models of the key polymer compounds and end groups were developed to study the luminescent characteristics of experimentally synthesized polyfluorenes. The structures of investigated copolymer models are shown in Fig. 6.

The problem to be solved in this work was to estimate the effect of the methods for covalent embedding of BT fragments in a polymer chain on PL of poly [(9,9-dioctylfluorene)-co-benzo [2,3,5] thiadiazole)]. Such a CPF can be synthesized in the Suzuki cross-coupling reaction (compound 1 in Fig. 1) [21]); in this case, a polymer chain cannot contain directly adjacent BT units. The model of a structural unit of such a CPF is the 4,7-bis(7-methyl-9,9-dioctyl-9H-fluorene-2-il)-2,1,3-benzo [2,3,5]thiadiazole trimer (**F-BT-F–C_8H_{17}** in Fig. 6).

Under Yamamoto polycondensation (compound 2 in Fig. 1) [21], blocks of several BT-units may be formed. The alkyl groups (–C_8H_{17}) were introduced in the CPFs during the monomer synthesis to obtain soluble polymers. The structures of the sequences of monomeric units in macromolecules with one or two BT units, namely **F-BT-F–C_8H_{17}** and **F-BT-BT-F–C_8H_{17}** (Fig. 6), were calculated using *ab initio* DFT optimization. For simplifying the quantum-chemical calculations, structural unit models with alkyl groups –C_8H_{17} substituted by a methyl group (**F-BT-F–CH_3**) were considered. In practice, the PL and EL properties of polymers are significantly affected by their end groups; therefore, the structure of models (Fig. 6) was changed by changing the methyl end group in F-BT-F–C_8H_{17} for the 4-methylphenyl group in **F-BT-F-2T-C_8H_{17}**.

The photophysical processes occurring upon electron density excitations were analyzed by the building of the highest occupied (**HOMO**) and the lowest unoccupied (**LUMO**) molecular orbitals presented in Fig. 7.

The shapes of the molecular orbitals (Fig. 7) unambiguously demonstrate that in the ground states of all four CPFs the electron density is delocalized over the entire fluorene chain and on the BT fragment. In the excited states, the electron density of occupied states is localized at the BT fragment. The partial electronic density attributed to sulfur

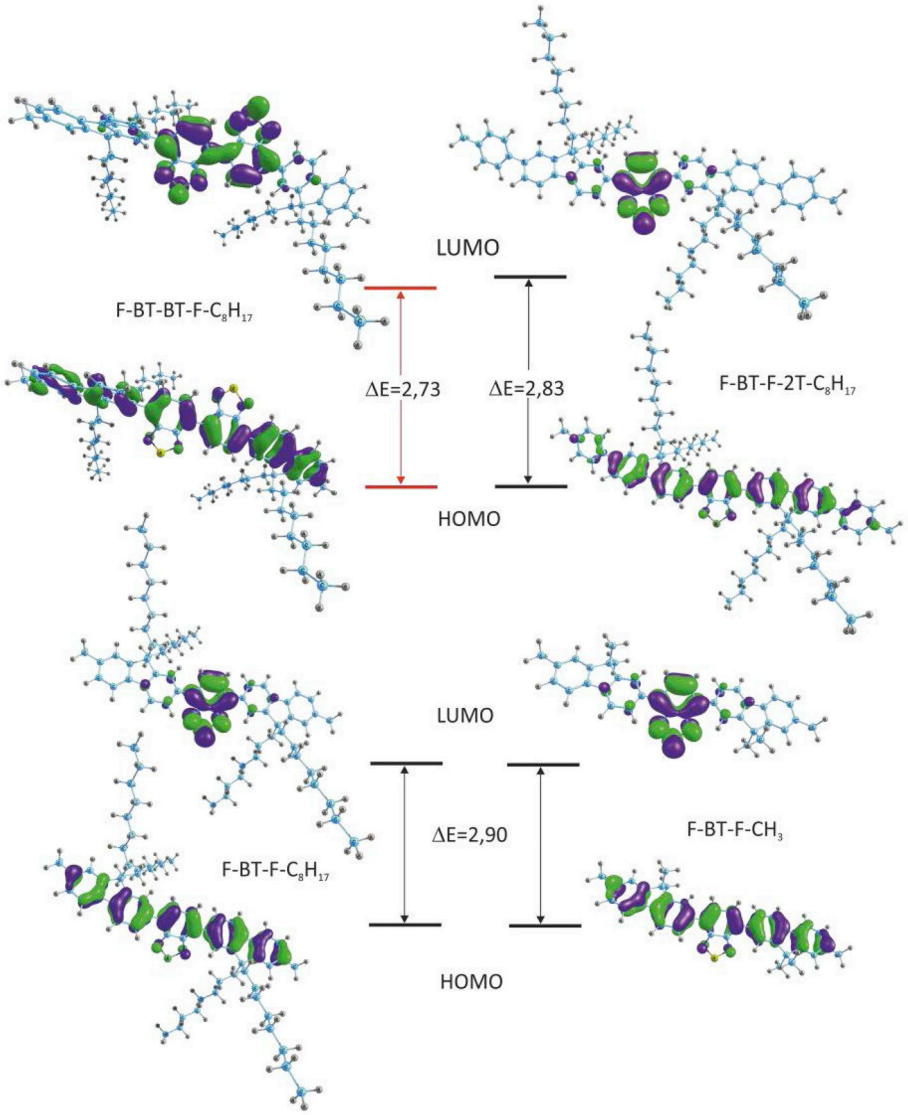

Fig. 7. Electron density distribution on the fluorene HOMO and LUMO: (F-BT-F—C_8H_{17}), (F-BT-F—CH_3), (F-BT-F-2T-C_8H_{17}), and (F-BT-BT-F—C_8H_{17}). ΔE_{Gap} is the energy difference between HOMO and LUMO (eV).

atoms contribute to the LUMO formation, being almost not involved in the HOMO formation.

Various alkyl substitutes, including C_8H_{17} and CH_3, are not involved in the MO formation. As was shown in Ref. [44] using the HF/6–31(p) technique, the presence of various alkyl groups does not affect the optical and electronic properties of CPFs. This is reflected also in the absorption spectra (Fig. 8), which are almost identical for the F-BT-F—C_8H_{17} and F-BT-F—CH_3 molecules. The wavelengths of the electronic transitions from S_0 to S_1 states are 504 and 501 nm, respectively.

Theoretical absorption spectra of CPFs F-BT-F-2T-C_8H_{17} and F-BT-BT-F—C_8H_{17} are presented in Fig. 8. Absorption spectrum of the CPF model with one BT fragment exhibits the maximum emission at 515 nm

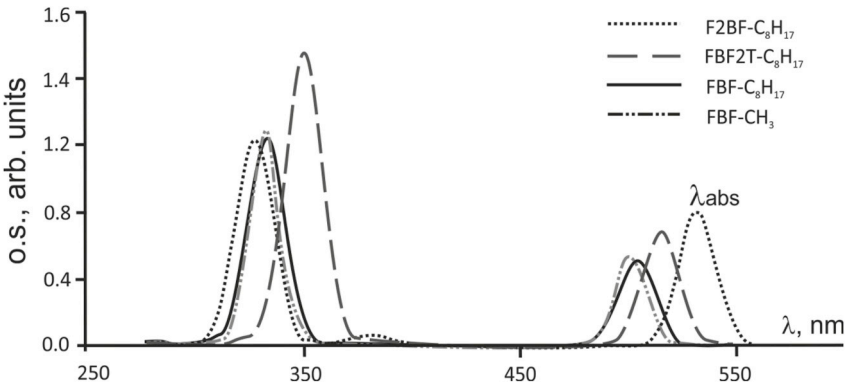

Fig. 8. Absorption spectra of model trimers F-BT-F—C_8H_{17} (black solid line), F-BT-F—CH_3 (grey dash-dot-dot line), F-BT-BT-F—C_8H_{17} (grey dotted line), and F-BT-F-2T-C_8H_{17} (grey long dash line). The structural models are shown in Fig. 2. O.S. denotes oscillator strength.

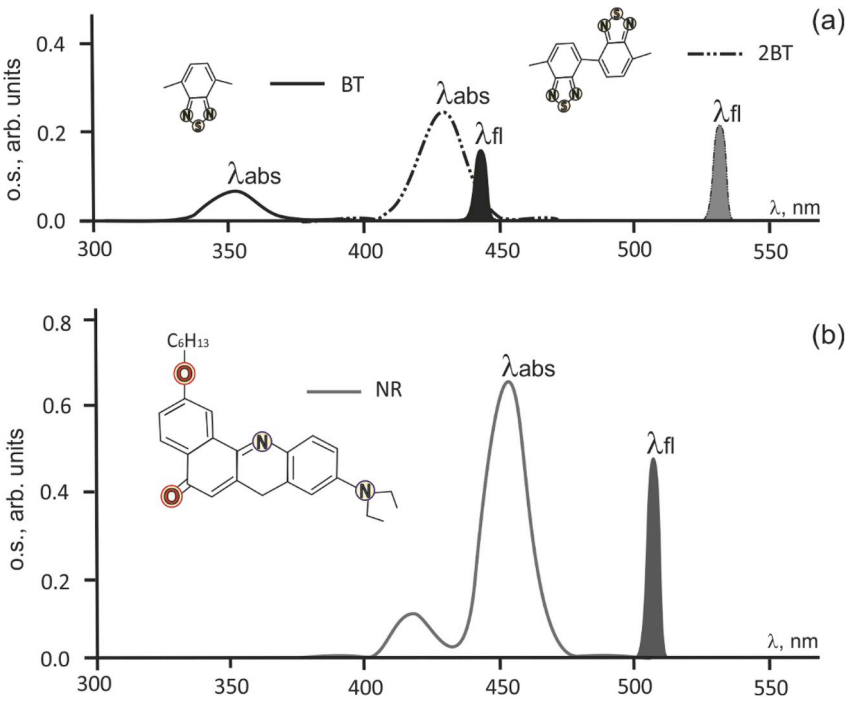

Fig. 9. Absorption spectra of the BT (black solid line), BT–BT grey dash-dot-dot line) chromophore groups at TD/B3LYP/6–31 (p, d) level of theory (**a**) and of the NR (grey solid line) group at PCM/TD/B3LYP/6–31 (p,d) calculation (**b**). Filled peaks correspond to the calculated emission wavelength. O.S. denotes oscillator strength.

Table 2
HOMO and LUMO energies and energy gaps (ΔE) of terfluorene tri- and tetramers at TD/B3LYP/6–31 (p, d) level of theory.

Energy, eV	Model polymer fragments			
	F-BT-BT-F−C_8H_{17}	F-BT-F-2T-C_8H_{17}	F-BT-F−C_8H_{17}	F-BT-F−CH_3
E_{LUMO}	−2.44	−2.27	−2.23	−2.24
E_{HOMO}	−5.17	−5.10	−5.13	−5.14
ΔE_{en}	2.73	2.83	2.90	2.90

(black solid line in Fig. 8), while in the model molecule containing two BT structural units, it is positioned in the long-wavelength spectral range, at 532 nm (grey dotted line in Fig. 8), which corresponds well to experimental **P1** and **P2** luminescence maxima at 540 and 575 nm, respectively (Fig. 4b, *cp.* curves 5 and 2). This fact can be explained by analyzing the TD-DFT absorption and emission spectra of individual BT molecules and BT dimers (Fig. 9a). At comparing the calculated absorption spectra of a BT monomer with BT dimer, there observes a bathochromic effect when the maximum at 353 nm changes to 429 nm, respectively. In the case of luminescence, the BT emission maximum is shifted from 443 to 531 nm of a BT dimer.

The solvent effect is of particular interest. So, in THF, the absorption and emission maxima for the BT dimer were found to be 360 and 442 nm, respectively, while for the F-BT-BT-F model, these values were 436 and 531 nm [45]. It was revealed that for the absorption and emission of a BT dimer under TD-DFT calculation at comparing with its absorption and emission in THF, there is a hypsochromic shift from 429 to 360 nm and 531 to 442 nm, respectively. The same tendency occurs for the F-BT-BT-F model by comparing the absorption spectra under TD-DFT and in THF: a blue shift is from 532 to 436 nm. For the F-BT-F absorption in $CHCl_3$, it occurs at shorter wavelengths at comparing with the TD-DFT absorption: the maximum at 420 nm (Fig. 5b, curve 4) and 515 nm, respectively. Thus, under the theoretical calculation, one needs correctly consider the change in environment to achieve better agreement between theory and experiment because of solvatochromism.

Therefore, the absorption spectrum of NR was calculated taking into account solvation effects in chloroform (PCM/TD/B3LYP/6–31 (p, d)) using PCM [31] (Fig. 9b). At PCM/TD/B3LYP/6–31 (p, d) level of theory, the absorption and emission wavelengths of HOMO-LUMO transition were found to be 455 and 505 nm, which is congruous to the experimental data. The maximum in the absorption band of NR in $CHCl_3$ occurs at 535 nm, and in the emission one at 600 nm (Fig. 5b, curves 2 and 7.) It also demonstrates that NR is extremely sensitive to the chemical nature of the environment, which can be used to tune the emission properties of fluorene-based polymers for chemosensor applications.

The HOMO and LUMO energies and energy gaps $\Delta E_{en} = E_{LUMO} - E_{HOMO}$ of F-BT-BT-F−C_8H_{17}, F-BT-F-2T-C_8H_{17}, and F-BT-F−CH_3 are presented in Table 2.

The alkyl group length does not affect the energy gap (Table 2). For example, the ΔE value for F-BT-F−CH_3 is the same as for F-BT-F−C_8H_{17}. An increase in the number of donor or acceptor groups almost does not influence the HOMO energy, since HOMO electron density is distributed over the entire CPF chain. However, the investigations of LUMO orbitals revealed a significant energy drop with increasing chain length, which facilitates a decrease in the energy gap. The lowest E_{LUMO} and, consequently, the smallest ΔE value are observed in the F-BT-BT-F−C_8H_{17} CPF (Table 2, Figs. 7 and 8) due to the fact that the electron density on the LUMO of all structures is localized on benzo [2,3,5] thiadiazole (Figs. 7 and 8) and in F-BT-BT-F−C_8H_{17} on two BT fragments.

3.2.2. End groups

Some end groups embedded in the LEP structure can significantly affect both chromatic coordinates and PL quantum yield. The same end group can influence different luminescent substances differently, e.g., actively quench the luminescence of one substance or not affect the luminescence of another. The electronic structure of the end groups and the nature of HOMO and LUMO orbitals determine the quenching trap mechanisms in light-emitting polymers.

Three types of the end groups were considered as as potential exciton traps (Fig. 10). The first group includes the simplest molecules End-1 (toluene) and End-2 (2-methyl-9,9-dioctyl-9H-fluorene)

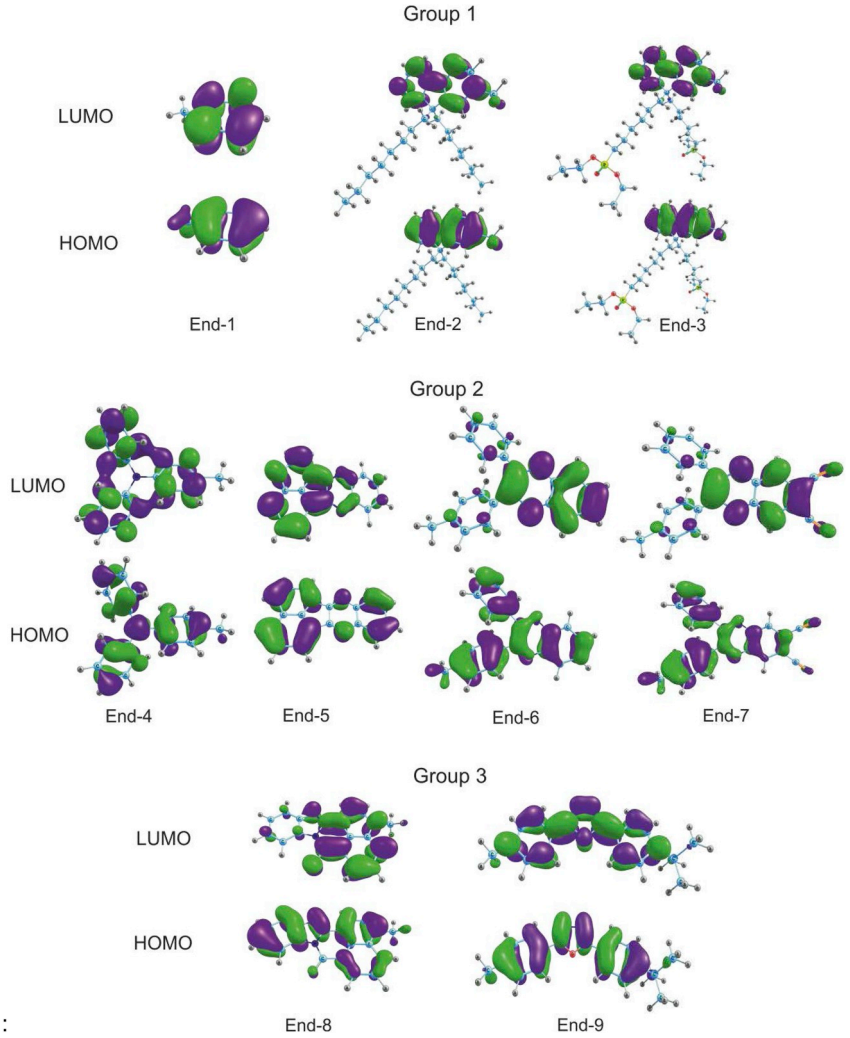

Fig. 10. Electron density distribution on the End-group HOMO and LUMO for End-1, End-2, End-3, End-4, End-5, End-6, End-7, End-8 and End-9 groups.

consisting of only carbon and hydrogen atoms, as well as the molecule End-3 (diethyl (6-{9-[6-(diethoxyphosphoryl)hexyl]-2-methyl-9H-fluoren-9-yl}hexyl)phosphonate) since the alkyl substitutes do not affect the electronic properties of the fluorene derivatives. The second group includes molecules End-4 (4-methyl-N,N-diphenylaniline), End-5 (3-methylacenaphthyleno [1,2-b]quinoxaline), End-6 (2-(4-methyl phenyl)-3-phenylquinoxaline), and End-7 (2-(4-methylphenyl)-3-phenyl quinoxaline-6,7-dicarbonitrile) of compounds containing nitrogen atom. The third group includes molecules End-8 (17-methyl-3,10-diazapentacyclo [$10.7.1.0^{2,10}.0^{4,9}.0^{16,20}$] icosa-1 (20),2, 4,6,8,12,14,16,18-nonaen-11-one) and End-9 (2-(4-tert-butylphenyl)-5-(4-methyl phenyl)-1,3,4-oxadiazole) containing two heteroatoms, oxygen and nitrogen (Fig. 10).

3.2.2.1. Group I. In the group End-1 in the ground state, all atoms of the molecule are involved in the HOMO formation, while the LUMO formation occurs almost without the participation of the alkyl CH_3 group. The HOMO-LUMO gap of End-1 molecule was 6.53 eV in contrast with the optical band which was found to be 7.14 eV due to optical (HOMO-1) - (LUMO + 1) electronic transition, rather than from HOMO – LUMO transition. At TD/B3LYP/6–31 (p, d) level of theory theoretical absorption spectrum for group End-1 has a peak at a wavelength of 174 nm (Fig. 11a). The calculated emission wavelength for this molecule is 181 nm (Fig. 11a).

The End-2 and End-3 electronic structures are very similar (Fig. 11a). In both cases, the HOMO and LUMO are localized at fluorene despite different alkyl substitutes which exhibit similar electronic properties. Analysis of theoretical absorption spectra at TD/B3LYP/6–31 (p, d) level of theory shows that they almost coincide. The emission wavelengths of these molecules are almost the same as well, 308 and 309 nm, respectively.

3.2.2.2. Group II. The benzene rings in the group End-4 are not coplanar (Fig. 12) with ground state HOMO and LUMO orbitals located at the same atoms (Fig. 10) with significant contribution of the nitrogen atom atomic orbitals to HOMO. The formation of the absorption peak at 306 nm (Fig. 11b) involves the electronic transitions from HOMO to LUMO and LUMO + 1 states.

For the End-4 group in S1 excited state, the interatomic bond distances change insignificantly with great change of the twisting angles of two aromatic rings relative to the third one with methyl substituent (Fig. 12).

At TD/B3LYP/6–31 (p, d) level of theory the luminescence wavelength of this end group is found to be 345 nm. This fact could explain large Stokes shift of End-4 substituted fluorone molecule.

The electron density of group-End-5 LUMO is shifted to the naphthal fragment. The absorption peak at 355 nm (Fig. 11b) corresponding to the transition from the HOMO to LUMO has a low intensity, in contrast to the peak with wavelength of 301 nm, which is responsible for the transition from the HOMO-1 to LUMO + 1. The calculated luminescence wavelength for this end group was found to be 393 nm, and the experimental value (curve 2, Fig. 6b) is 480 nm.

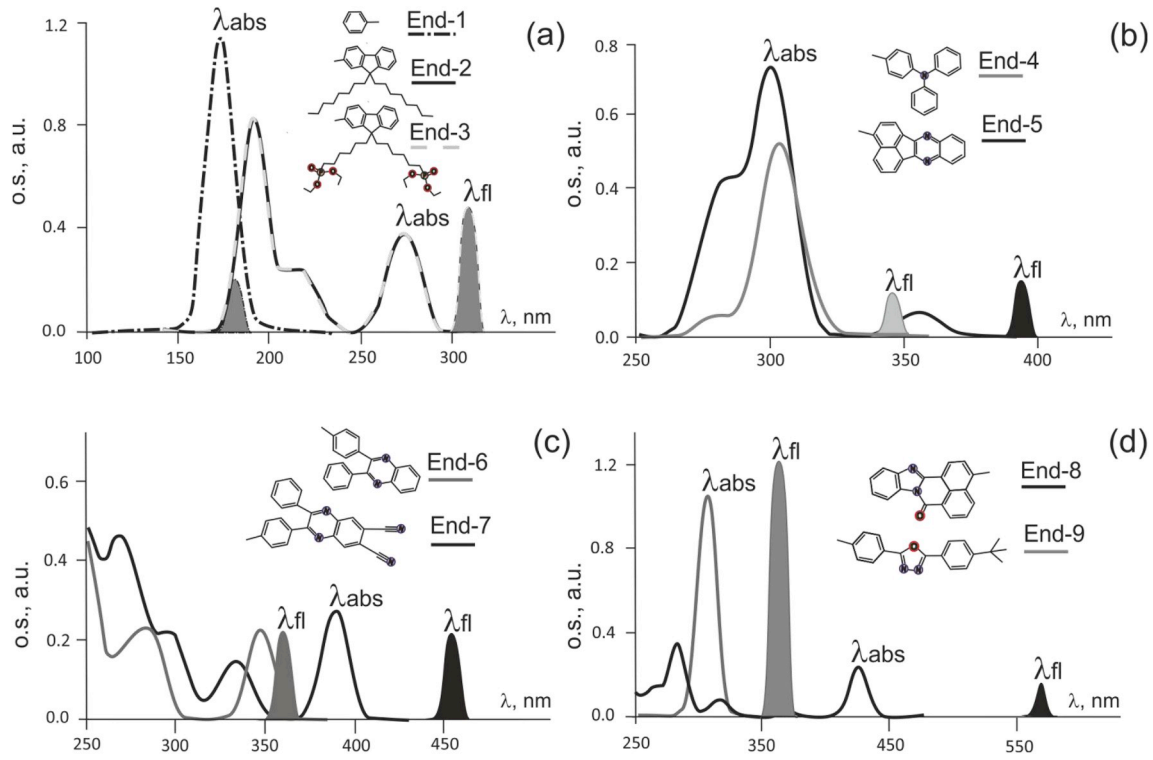

Fig. 11. Absorption and luminescence spectra of End groups End-1, End-2, and End-3 (**a**); End-4 and End-5 (**b**); End-6 and End-7 (**c**); End-8 and End-9 (**d**) at TD/B3LYP/6–31 (p, d) level of theory. Filled peaks correspond to the calculated radiation wavelength.

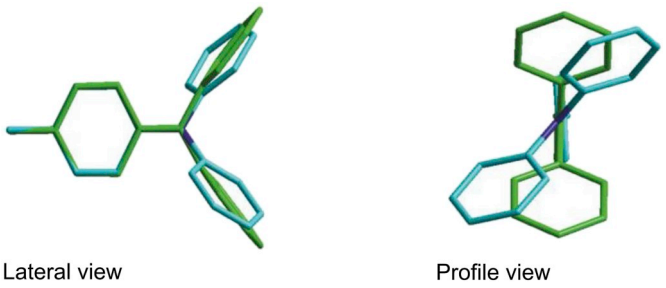

Fig. 12. Atomic structure of group End-4 in the ground (blue) and excited (green) states. (For interpretation of the references to color in this figure legend, the reader is referred to the Web version of this article.)

Slight differences in atomic structure of End-6, and End-7 substitutes lead to visible differences in their optical properties. Both End-6 and End-7 luminescence and absorption spectra demonstrate similarities in the peak shapes and intensities with large red shift (93 nm) of End-7 luminescence spectrum (Fig. 11c) in respect to End-6 one. The emission wavelengths of the end groups are 360 and 453 nm, respectively. In the experiment, there is a maximum for P10 with R_7 (Fig. 6b, curve *3′*) in the luminescence band at 580 nm. The End-6 and End-7 HOMO orbitals (Fig. 10) are delocalized at entire molecules. In the case of End-7, HOMO includes two N atoms as *p*-type nonbonding orbitals. In the End-6 and End-7 LUMO, the electron density is localized at the quinoxaline core with almost zero contributions of two phenyl substituents. In S1 excited state, these end groups are characterized by noticeable changes in the bond lengths within the diaza-benzene ring.

3.2.2.3. Group III. In End-8 and End-9 molecules, the HOMOs are formed with the participation of two nitrogen atoms, while oxygen p_z electrons in End-8 are not involved in the chemical bond formation (the bottom of Fig. 10). In End-9, the LUMO is formed with almost all atoms involved. Both End-8 and End-9 luminescence and absorption spectra (Fig. 11, bottom right) differ due to the structural features of the molecules. For End-9, a highly intense peak in absorption is observed at 307 nm with almost the same oscilator strength of luminescence peak at 362 nm. End-8 also reveals close oscilator strengths for absorption and emission spectra (Fig. 11). The group End-8 in the excited state undergoes changes in almost all bond lengths. Theoretical absorption wavelength was found to be 425 nm, which corresponds well to maximum intensity of experimental absorption band of R_3-F-R_3 in chloroform at 415 nm (green curve 6, Fig. 4b). Theoretical luminescence peak is found at 570 nm which corresponds to broad luminescence band at 480–600 nm (curve *5,* Fig. 4b) with the intensity maximum at 510 nm and a shoulder at 540 nm. In S1 excited state, the End-9 substituent is characterized by elongation of the C—N bond lengths in oxadiazole cycle about 0.053 Å. The visible changes in the bond lenghs are caused by the electronic transition from bonding HOMO to antibonding LUMO which are formed mostly by the atomic orbitals of carbon and nitrogen atoms (Fig. 10). HOMO-LUMO electronic transition causes shortening of the nitrogen–nitrogen bond from 1.388 Å length (single bond in the ground state) to 1.327 Å (sesquialteral bond in exited state). The emission wavelength for the End-9 substituent at TD/B3LYP/6–31 (p, d) level of theory is 362 nm (Fig. 11d).

Table 3 presents comparative data on the HOMO and LUMO energies and energy gaps for the end groups of three types in the isolated state with disregard of conjugation with the fluorene units. In particular, analysis of E_{LUMO} values of End groups in comparison with CPF ones in the region of −2.44 and −2.23 eV suggests that the emission quenching is facilitated by the end groups with E_{LUMO} higher the CPF ones. During electronic transport an exited electron can either return back to its parent HOMO with emission of a photon or to suffer non-radiative transition to HOMO of a quencher, which could be energetically preferable.

Table 3
The HOMO and LUMO values and energy gaps for the end groups.

Parameter	Group 1			Group 2				Group 3	
	End-1	End-2	End-3	End-4	End-5	End-6	End-7	End-8	End-9
E_{LUMO}, eV	0.21	−0.59	−0.64	−1.94	−0.20	−1.77	−2.78	−2.35	−1.38
E_{HOMO}, eV	−6.32	−5.48	−5.53	−5.91	−4.79	−5.86	−6.46	−5.66	−5.83
ΔE_{energy}, eV	6.53	4.89	4.89	3.97	4.59	4.09	3.68	3.31	4.45

4. Conclusions

Both experimental findings and theoretical consideration of optical properties of CPFs reveal the important role of intra- and intermolecular interactions, including solvent effects caused by solvent molecules and electronic cooperations along the polymer chains. A set of copolyfluorenes were synthesized using Suzuki and Yamamoto reactions. It was found that the differences between the photo- and electroluminescent properties of CPFs are caused by the formation of microblock structures of luminophore comonomer units in Yamamoto case, which it is observed even at 1-mol% content of comonomer units. The Yamamoto approach results in formation of a new LEP based on 1,4-dibromobenzo [2,3,5]thiadiazole comonomer entering the polymer backbone and a deterioration of the conditions of energy transfer from fluorene units to the chromophore or the chromophore located in the polymer pendant. The quantum-chemical calculations of atomic structure and emission and absorption spectra at B3LYP/6–31 (p, d) and TD/B3LYP/6–31 (p, d) levels of theory confirm the key experimental results.

The microwave irradiation increases the rate of CPF synthesis by the factor of 10. Embedding of 2.5–10 mol% of 3,6-Cz comonomer units in the backbone improves the solubility and reduces the CPF structurization in films: the fraction of β-phase diminishes.

It was shown that conjugation of nitrile substituted quinoxaline end groups with fluorene yelds the yellow-red luminescence of CPF films. Attachment of the quinoxaline end groups through the naphthal fragment leads to the green luminescence, whereas the conjugation through the benzene ring does not change the coordinates of blue polyfluorene luminescence. In the first two cases, the high-efficiency energy transfer from fluorene to the quinoxaline group is observed in condenced phase.

Data availability

The raw/processed data required to reproduce these findings cannot be shared at this time as the data also forms part of an ongoing study. Data will be made available on request.

Acknowledgments

The quantum yield measurements were performed at the Center for Optical and Laser Materials Research, St. Petersburg State University. P. Avramov gratefully acknowledges the financial support of National Research Foundation of Republic of Korea under Grant No. NRF-2017R1A2B4004440. This work has been carried out using computing resources of the federal collective usage center Complex for Simulation and Data Processing for Mega-science Facilities at NRC “Kurchatov Institute”, < http://ckp.nrcki.ru > .

Appendix A. Supplementary data

Supplementary data to this article can be found online at https://doi.org/10.1016/j.polymer.2019.02.015.

References

[1] M.F. Jared, J.J. Intemann, M. Cai, T. Xiao, R. Shinar, J. Shinar, M. Jeffries-El, Polym. Chem. 2 (2011) 2299–2305.
[2] J. Kim, D. Khim, R. Kang, S.-H. Lee, K.-J. Baeg, M. Kang, Y.-Y. Noh, D.-Y. Kim, Simultaneous enhancement of electron injection and air stability in N-type organic field-effect transistors by water-soluble polyfluorene interlayers, ACS Appl. Mater. Interfaces 6 (11) (2014) 8108–8114, https://doi.org/10.1021/am500466q.
[3] S. Donets, A. Pershin, S.A. Baeurle, Computation of full polymer-based photovoltaic nanodevices using a parametrized field-based multiscale solar-cell approach, Org. Electron. 22 (2015) 216–228 https://doi.org/10.1016/j.orgel.2015.03.049.
[4] H. Liu, L. Hu, F. Wu, L. Chen, Y. Chen, Polyfluorene electrolytes interfacial layer for efficient polymer solar cells: controllably interfacial dipoles by regulation of polar groups, ACS Appl. Mater. Interfaces 8 (15) (2016) 9821–9828, https://doi.org/10.1021/acsami.6b00637.
[5] U. Scherf, U. Scherf, D. Neher (Eds.), Polyfluorenes, Springer, Berlin, 2008.
[6] L. Zhao, S. Wang, S. Shao, J. Ding, L. Wang, X. Jing, F. Wang, Stable and efficient deep-blue terfluorenes functionalized with carbazole dendrons for solution-processed organic light-emitting diodes, J. Mater. Chem. C 3 (2015) 8895–8903, https://doi.org/10.1039/C5TC01711D.
[7] F. Huang, X. Wang, D. Wang, W. Yang, Y. Cao, Synthesis and properties of a novel water-soluble anionic polyfluorenes for highly sensitive biosensors, Polymer 46 (2005) 12010–12015 https://doi.org/10.1016/j.polymer.2005.10.034.
[8] K.-T. Wong, Y.-Y. Chien, R.-T. Chen, C.-F. Wang, Y.-T. Lin, H.-H. Chiang, P.-Y. Hsieh, C.-C. Wu, C.H. Chou, Y.O. Su, G.-H. Lee, S.-M. Peng, Ter(9,9-diarylfluorene)s: highly efficient blue emitter with promising electrochemical and thermal stability, J. Am. Chem. Soc. 124 (2002) 11576–11577, https://doi.org/10.1021/ja0269587.
[9] W. Dong, S. Xue, P. Lu, J. Deng, D. Zhao, C. Gu, Y. Ma, Functionality of peripheral side chain for enhanced performance of conjugated polymer—F8BT as an example, J. Polym. Sci. Polym. Chem. 49 (2011) 4549–4555 https://doi.org/10.1002/pola.24898.
[10] J. Liu, L. Chen, S. Shao, Z. Xie, Y. Cheng, Y. Geng, L. X. Wang, X. B. Jing, F. S. Wang, Three-color white electroluminescence from a single polymer system with blue, green and red dopant units as individual emissive species and polyfluorene as individual polymer host, Adv. Mater. 19 (2007) 4224–4228, https://doi.org/10.1002/adma.200701104.
[11] V.M. Svetlichnyi, E.L. Aleksandrova, N.V. Matyushina, L.A. Myagkova, T.N. Nekrasova, R.Yu Smyslov, Molecular design of optoelectronic structures based on carbazole- and indolocarbazole-containing polyphenylquinolines, High Perform. Polym. 29 (6) (2017) 730–749, https://doi.org/10.1177/0954008317706734.
[12] N. Fu, Y. Wang, D. Liu, C. Zhang, S. Su, B. Bao, B. Zhao, L. Wang, A conjugated polyelectrolyte with pendant high dense short-alkyl-chain-bridged cationic ions: analyte-induced light-up and label-free fluorescent sensing of tumor markers, Polymers 9 (227) (2017) 1–14, https://doi.org/10.3390/polym9060227.
[13] G.I. Nosova, D.A. Lypenko, R.Yu Smyslov, I.A. Berezin, E.V. Zhukova, E.I. Mal’tsev, A.V. Dmitriev, L.S. Litvinova, N.A. Solovskaya, O.V. Dobrokhotov, I.G. Abramov, A.V. Yakimanskii, Synthesis and photo- and electroluminescent properties of copolyfluorenes with nile red fragments in side chains, Polym. Sci. B 56 (1) (2014) 59–76 https://doi.org/10.1134/S1560090414010072.
[14] F. Pschenitzka, J.C. Sturm, Three-color organic light-emitting diodes patterned by masked dye diffusion, Appl. Phys. Lett. 74 (1999) 1913–1915 https://doi.org/10.1063/1.123711.
[15] Y.S. Park, S.J. Park, W. Shin, B. Lee, B. Jung, J.H. Kim, Synthesis and characterization of di-hexyl-fluorene and triphenylamine based copolymers containing 1,3,4-oxadiazole pendants, Mol. Cryst. Liq. Cryst. 538 (1) (2011) 118–126 https://doi.org/10.1080/15421406.2011.563673.
[16] C.W. Huang, K.Y. Peng, C.Y. Liu, T.H. Jen, N.J. Yang, S.A. Chen, Creating a molecular-scale graded electronic profile in a single polymer to facilitate hole injection for efficient blue electroluminescence, Adv. Mater. 20 (2008) 3709–3716, https://doi.org/10.1002/adma.200800109.
[17] O.V. Mikhnenko, M. Kuik, J. Lin, N. van der Kaap, T.-Q. Nguyen, P.W.M. Blom, Trap-limited exciton diffusion in organic semiconductors, Adv. Mater. 26 (2014) 1912–1917, https://doi.org/10.1002/adma.201304162.
[18] A.J.C. Kuehne, A.R. Mackintosh, R.A. Pethrick, β-phase formation in a crosslinkable poly(9,9-dihexylfluorene), Polymer 52 (2011) 5538–5542, https://doi.org/10.1016/j.polymer.2011.09.044.
[19] M. Knaapila, D.W. Bright, B.S. Nehls, V.M. Garamus, L. Almasy, R. Schweins, U. Scherf, A.P. Monkman, Development of intermolecular structure and beta-phase of random poly [9, 9-bis (2-ethylhexyl) fluorene]-co-(9, 9-dioctylfluorene) in methylcyclohexane, Macromolecules 44 (2011) 6453–6460, https://doi.org/10.1021/ma201250h.
[20] Y. Deng, W. Yuan, Z. Jia, G. Liu, H- and J-aggregation of fluorene-based chromophores, J. Phys. Chem. B 118 (2014) 14536–14545, https://doi.org/10.1021/jp510520m.
[21] N.P. Yevlampieva, A.P. Khurchak, G.I. Nosova, R. Yu Smyslov, I.A. Berezin,

D.M. Ilgach, T.N. Kopylova, R.M. Gadirov, A.V. Yakimansky, Chain microstructure and specific features of excitation energy transfer in solution and films of poly(9,9-dioctylfluorene) doped with 2,1,3-benzothiadiazole comonomer units, Chem. Phys. Lett. 645 (2016) 100–105 https://doi.org/10.1016/j.cplett.2015.12.039.
[22] P.-I. Lee, S.L.-C. Hsu, R.-F. Lee, Polymer 48 (2007) 110.
[23] I.G. Abramov, A.V. Smirnov, M.B. Abramova, R.S. Begunov, L.S. Kalandadze, O.V. Smirnova, V.V. Plakhtinskiy, Izvestiya vysshikh uchebnykh zavedeniy khimiya khimicheskaya tekhnologiya 44 (6) (2001) 134 In Russian http://journals.isuct.ru/ctj/.
[24] G.I. Nosova, L.S. Litvinova, I.A. Berezin, E.V. Zhukova, R. Yu Smyslov, A.V. Yakimansky, Microwave synthesis of polyfluorenes and copolyfluorenes and their optical properties, Polym. Sci. B 61 (2019) 8–19, https://doi.org/10.1134/S1560090419010081.
[25] D. Bondarev, J. Zedník, Influence of covalent structure and molecular weight distribution on the optical properties of alternating copolymers and oligomers with 1,2,3-triazole and 1,3,4-oxadiazole side group, Polymer 124 (2017) 107–116 https://doi.org/10.1016/j.polymer.2017.07.045.
[26] J.C. DeMello, H.F. Wittmann, R.H. Friend, An improved experimental determination of external photoluminescence quantum efficiency, Adv. Mater. 9 (1997) 230–232.
[27] C. Lee, W. Yang, R.G. Parr, Development of the Colle-Salvetti correlation-energy formula into a functional of the electron density, Phys. Rev. B 37 (1988) 785–787.
[28] A.D. Becke, Density-functional exchange-energy approximation with correct asymptotic behavior, Phys Rev A 38 (1988) 3098–3105.
[29] P.C. Hariharan, J.A. Pople, The influence of polarization functions on molecular orbital hydrogenation energies, Theoretica Chimica Acta 28 (3) (September 1973) 213–222.
[30] P. Hohenberg, W. Kohn, Inhomogeneous electron gas, Phys. Rev. Lett. 136 (1964) B864-B88.
[31] B. Mennucci, J. Tomasi, Continuum solvation models: a new approach to the problem of solute's charge distribution and cavity boundaries, J. Chem. Phys. 106 (12) (1997 Mar 22) 5151–5158.
[32] M.W. Schmidt, K.K. Baldridge, J.A. Boatz, S.T. Elbert, M.S. Gordon, J.H. Jensen, S. Koseki, N. Matsunaga, K.A. Nguyen, S. Su, T.L. Windus, M. Dupuis, J.A. Montgomery, General atomic and molecular electronic structure system, J. Comput. Chem. 14 (1993) 1347–1363.
[33] J.-F. Lee, S.L.-C. Hsu, Polymer 50 (2009) 5668.
[34] A. Monkman, C. Rothe, S. King, F. Dias, Polyfluorene. Photophysics, Adv. Polym. Sci. 212 (2008) 187–225.
[35] M. Grell, D.D.C. Bradley, X. Long, T. Chamberlain, M. Inbasekaran, E.P. Woo, M. Soliman, Acta Polym. 49 (1998) 439.
[36] J. Ishii, T. Sunaga, S. Deguchi, M. Ttsukioka, High Perform. Polym. 21 (2009) 393.
[37] A. Sergent, G. Zucchi, R.B. Pansu, M. Chaigneau, B. Geffroy, D. Tondelier, M. Ephritikhine, J. Mater. Chem. C 1 (2013) 3207–3216.
[38] D.W. Bright, F.B. Dias, F. Galbrecht, U. Scherf, A.P. Monkman, Adv. Funct. Mater. 19 (2009) 67–73.
[39] C.W. Cone, R.R. Cheng, D.E. Makarov, D.A. Vanden Bout, J. Phys. Chem. B 115 (2011) 12380–12385.
[40] J.H. Cook, J. Santos, H.A. Al-Attar, M.R. Bryce, A.P. Monkman, J. Mater. Chem. C 3 (2015) 9664.
[41] C. Xia, R.C. Advincula, Macromolecules 34 (17) (2001) 5854.
[42] M. Knaapila, A.P. Monkman, Adv. Mater. 25 (2013) 1090.
[43] G. Klaerner, R.D. Miller, Macromolecules 31 (1998) 200.
[44] M. Belletête, S. Beaypré, J. Bouchard, P. Blondin, M. Leclerc, G. Durocher, J. Phys. Chem. B 104 (2000) 9118.
[45] P. Anant, N.T. Lucas, J. Jacob, Org. Lett. 10 (24) (2008) 5533.